Synthesis and Characterization of Ba doped Bismuth Sodium Titanate (BNT)

Thesis submitted in partial fulfillment of the requirement for the award of

Degree of

Masters of Science

In

Physics

Submitted By

Kaifi Sehgal

Reg. No. 301404009

Under the supervision of

Dr. Poonam Uniyal

Assistant Professor

July, 2016

DEPARTMENT OF PHYSICS AND MATERIALS SCIENCE

THAPAR UNIVERSITY

PATIALA, PUNJAB

CERTIFICATE

This is to certify that this dissertation entitled "Synthesis and Characterization of Ba doped Bismuth Sodium Titanate (BNT)'' is submitted by Kaifi Sehgal (Roll. No. 301404009) in the fulfilment of the requirement for the award of degree of Masters of Science in Physics from School of Physics and Materials Science, Thapar University, Patiala (Punjab), India. It is an exclusive record of candidate's own research under the supervision of Dr. Poonam Uniyal. This dissertation in part or full has not been submitted in any other institution for the award of such kind of degree.

Dr. Poonam Uniyal

(Supervisor)

Assistant Professor

School of Physics and Materials Science

Thapar University, Patiala

Countersigned by:

Dr. M. K. Sharma

Professor and Head of Department

School of Physics and Materials Science,
Thapar University, Patiala

Dr. S. S. Bhatiya

Dean of Academic Affairs

Thapar University, Patiala

ACKNOWLEDGEMENT

I am submitting my dissertation for the fulfilment of my 'M.Sc.' degree. This work would not have been accomplished without the support, help and guidance of a large number of people. I express my deep gratitude and respect to my supervisor **Dr. Poonam Uniyal** (Assistant Professor, School of Physics and Materials Science) for his keen interest, strong motivation and constant encouragement during the course of the work. I thank him for his great patience, constructive criticism and myriad useful suggestions apart from invaluable guidance to me.

I would also like to thank **Dr. Manoj Kumar Sharma** (Head of Department) and the entire esteem faculty members of School of Physics and Materials Science for their constructive suggestions at different stages of this work.

I would like to thank to **Mrs. Manpreet Kaur and Mr. Manjinder Singh** for their patience, love, moral support and constant co-operation whenever I required.

The meaning of my life and work is incomplete without paying regards to my respected parents whose blessings and continuous encouragement have shown me the path to achieve my goals.

And above all, I pay my regards to the Almighty for His blessings.

Kaifi

Kaifi Sehgal

Dedicated to my loving parents

ABSTRACT

Oxide materials with perovskite structure having the general formula ABO_3, form the backbone of the ferroelectrics industry. For a long time, ferroelectric materials have come into widespread use in applications that range in sophistication from medical, ultrasound and underwater sonar systems, smoke detector buzzers to novel applications in active and passive damping systems for sporting goods and automobile and aerospace sectors. However, an attention has been focused across the globe to find out new environment-friendly lead-free ferroelectric materials. The $(Bi_{0.5}Na_{0.5})$ TiO_3 (BNT) based composition is reported as the promising for piezoelectric applications. Application of BNT into practical devices has been hindered by leakage problems that lead to low resistivity. In order to reduce the problems mentioned here, the method of forming binary solid solutions with other perovskites with good dielectric properties was adopted.

Bismuth Sodium Titanate ($Na_{0.5}Bi_{0.5}TiO_3$) was prepared by sol gel autocombustion method. Calcination of the sample prepared through sol gel method was done at 750°C for 10 hours. XRD of the samples was done in which a single perovskite phase was confirmed. The samples were sintered using the conventional sintering method at 780°C for 10 hours. SEM images of the samples were taken which showed dense microstructure and uniform grain size. Comparative study of dielectric properties of the samples was done. PE loop measurements were done to confirm the ferroelectric nature of the sample.

TABLE OF CONTENTS

List of Figures

List of Tables

CHAPTER 1: INTRODUCTION

1.1 Introduction

In recent times, the human race is behind the development of technology for their better livelihood. They are actively participating to hunt for superior and smarter materials to accomplish these technological desires. In order to design a material for specific application, numerous research groups are involved with only aim to design a material which may lead to significant advancement in miniaturizing of electronic components. In this scenario, the perovskites having ABO_3 type structure got excessive attention from various scientists, in last few decades [1-2]. These materials exhibit variety of functional properties for industrial applications. Ferroelectric materials are one of the unique class of perovskites. Basically, the ferroelectric materials show reversible spontaneous polarization by applying electric field, which was discovered by Rochelle salt in 1921.

Most of the ferroelectric materials are lead based which are dominantly used in sensors, actuators, transducers, medical, ultrasound and many more electronics devices. The lead based materials possess superior piezoelectric, dielectric and electromechanical properties [4-5]. However, the major disadvantage of these perovskites is their toxicity [6]. Generally, the lead based materials contain more than 60% of lead, which can interact with environment while processing and disposal. As the lead is absorbed by human causes severe problems to nerve pulse transmission, heart activity, blood clotting and disturbs the working of brain neurotransmitter. Also, it is very problematic to remove lead from human organisms [7]. In addition, for biosensing applications the material should be biocompatible with human body. To circumvent the toxicity of lead materials, it is essential to develop an alternate. The increasing demand of lead free ferroelectric materials in daily life necessitate development of novel materials with high dielectric constant, low dielectric loss, good piezoelectricity and pyroelectric properties. Consequently, intensive research has been carried out to search appropriate lead free perovskites materials all around the globe.

Among all the lead free ceramics (Bi, Na) TiO_3 based ceramics are considered to be good candidates because of it strong ferroelectricity. The BNT ceramics exhibit rhombohedral symmetry and was first discovered by Smolenski and his co-workers in 1961 [8]. BNT emerges as a suitable alternate for lead based actuators. Numerous studies have been conducted so far to investigate properties of BNT synthesized from different methods such as solid state method, sol-gel method, chemical vapour deposition and hydrothermal method. The synthesis method of BNT plays a crucial role in order to determine the particle size that affect various properties. Synthesis of BNT through auto-combustion method, using glycine as fuel, is a new way of controlling particle size. This synthesis route is advantages as it offers better homogeneity, low temperature synthesis, inexpensive, ease of fabrication and fine sized powder production [9-10]. So, there is need of a systematic study to investigate the properties of BNT synthesized from auto-combustion method.

1.2 Structure of Perovskites

The unit cell of perovskite consists of eight large A^{a+} ions, one small B^{b+} ion, and six O^{2-} ions. The valences "a" and "b" range from 1 to 3, and 3 to 6, respectively [11]. The perovskite unit cell can be pictured as a face centred cubic structure, where the A^{a+} ions sit on the corners of the unit cell, and the O^{2-} ions sit on the faces of the unit cell. The B^{b+} ion occupies the octahedral interstitial site. The A-site ions are coordinated by 12 O^{2-} ions, while the B-site ion is coordinated by six O^{2-} ions [12]. At elevated temperatures, the perovskite structure becomes cubic. Each atom at the cube corner is shared by eight other cubes, while the atoms at the center of the cube face are shared by two cubes. Hence, only 1/8 of each A cations and ½ of each oxygen atom actually belong to the cube shown in Fig. 1.1. Currently, there are hundreds of compositions having ABO_3 formula.

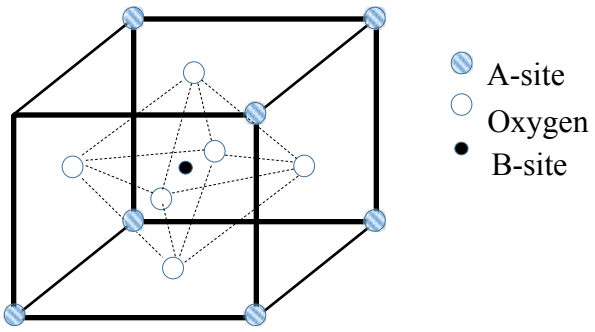

Figure 1.1: Structure of perovskites.

1.3 Ferroelectrics

Ferroelectricity was discovered in 1920 in Rochelle salt by Valasek. Ferroelectricity is a property of dielectric material that show spontaneous electric polarization that can be reversed in direction by the application of an external electric field [15]. In ferroelectric crystals the positive and negative centers do not coincide. Also, the plot between the polarization and electric field for ferroelectric crystal shows a hysteresis loop.

1.3.1 Types of ferroelectric

On the basis of frequency dependence of ε_r ferroelectric materials can be classified as normal or relaxor ferroelectrics.

i. Normal ferroelectrics: At Curie temperature T_C, normal ferroelectrics show either first or second transition. They obey Curie Weiss law and show weak frequency dependence. As compared to relaxor ferroelectric they exhibit large remanent polarization. They do not show hysteresis loop about T_C.

ii. Relaxor ferroelectrics: At Curie maxima, they show a broad diffuse transition. They obey curie Weiss square law and show strong frequency dependence. As compared to normal ferroelectrics they show a weak remanent polarization.

They show a hysteresis loop about T_C [16].

1.4 Properties of ferroelectric

1.4.1 Crystal symmetry

Every crystal can be classified by 230 crystallographic space groups, i.e., symmetry classes. The point group are only 32 as compared to the space group. Their classification in detail is given below in the figure 1.2.

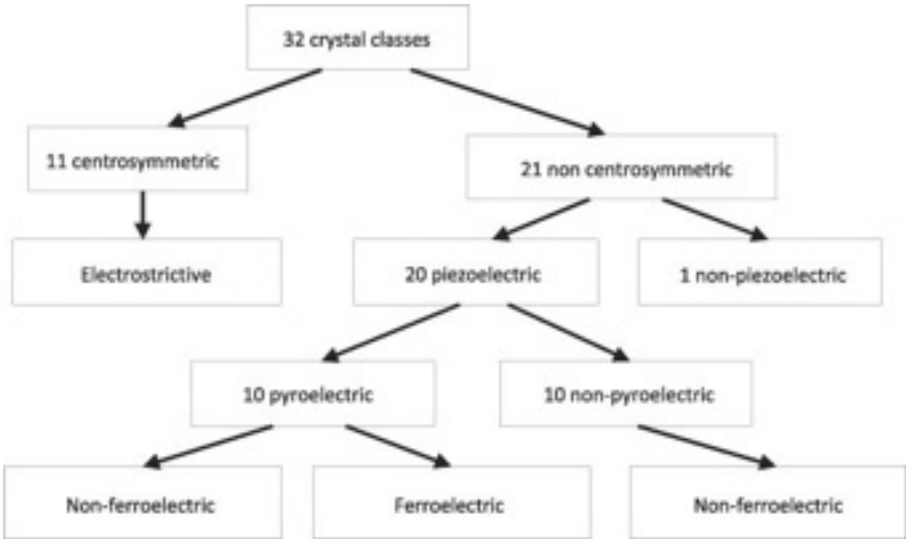

Figure 1.2: Flow chart showing the division of the 32-point group.

1.4.2 Dielectric

A dielectric material is basically an electrical insulator that can be polarized by an applied electric field. When a dielectric material is placed in an electric field, the electric charges do not flow through it, but only shift from average equilibrium positions causing dielectric polarization. This leads to displacement of positive charges towards the field and negative charges in the opposite direction. It creates an internal electric field which reduces the overall field within the dielectric. The amount of polarization produced is given by dimensionless quantity called dielectric constant.

1.4.2.1 Frequency dependence of dielectric

With increasing frequency, the dielectric constant of a dielectric material goes on decreasing. At low frequencies, the dielectric loss is mainly because of dc resistivity. However, the dielectric loss at high frequencies is mainly because of ionic transition from lower energy state to higher energy state or because of dipole rotations. Due to upward transition, the energy absorbed is from the applied field. The energy absorption is only possible, when the permanent dipole moments and orientational polarization are present [13].

1.4.2.2 Dielectric relaxation

Maximum value of polarization for the dielectric material can be achieved by taking a finite amount of time. This occurs because of the force between adjacent molecules which tends to prohibit the alignment along the external field. This process is known as dielectric relaxation. It is a latent property of relaxor ferroelectrics [14].

1.4.3 Polarization

When we place a dielectric material in an electric field, the positive and negative charges of the material are displaced from their equilibrium position by very small distance throughout the volume of dielectric as depicted in figure 1.3. This will lead to the formation of large number of dipoles each having some dipoles in the direction of field and the material is said to be polarized with polarization vector P. The dipole moment per unit volume is defined as polarization.

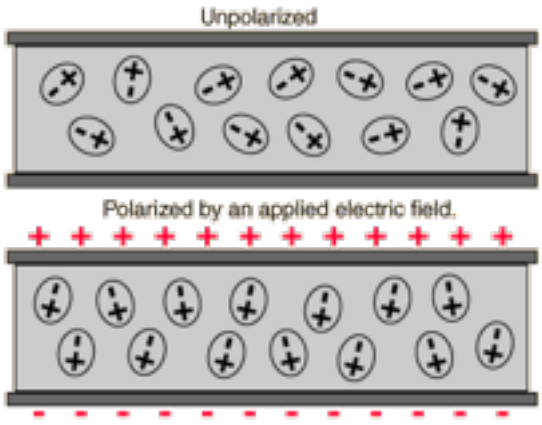

Figure 1.3: The process of polarization.

i. *Electronic polarization:*

The electronic polarization occurs due to the displacement of the electron cloud of an atom with respect to its nucleus in the presence of applied electric field. At optical frequencies, polarization and the dielectric constant of material results mainly from electronic polarization.

ii. *Ionic polarization:*

The ionic polarization occurs due to the displacement of a charged ions with respect to the other ions in the solid. At low temperature, ionic contribution becomes more important.

iii. *Dipolar polarization:*

The dipolar polarization occurs due to the polar substance which can orient themselves in the presence of an external electric field. The thermal agitation of the molecules tends to prevent the ordering effect of electric field. When the different dipoles make all possible angles varying from zero to π in the direction of field, the equilibrium stage is reached.

iv. *Space charge polarization:*

This polarization occurs due to the accumulation of charges at the interface or at the grain boundary of the polycrystalline material. In response to the applied field the

ions diffuse over observable distances giving rise to the re-distribution of charges in the dielectric medium.

1.4.4 P-E Hysteresis loop

A polarization-electric field loop (P-E loop) is a hysteretic curve showing the variation of electric polarization (Coulombs per square meter) with electric field (Volts per meter). The P-E curve is not monotonic but history dependent in that the current value of the polarization depends on the current and previous values of the electric field. By convention, P and E point along the same direction which is taken to be a crystallographic axis. In principle, however, polarization and electric field are both vectors so that P-E curves could be prepared with the vectors pointing in different directions. Also it is generally assumed that the stress is zero in P-E loops. Alternate curves could be prepared for different stress states giving a family of hysteretic curves.

The P-E hysteresis curve is shown in fig 1.4.

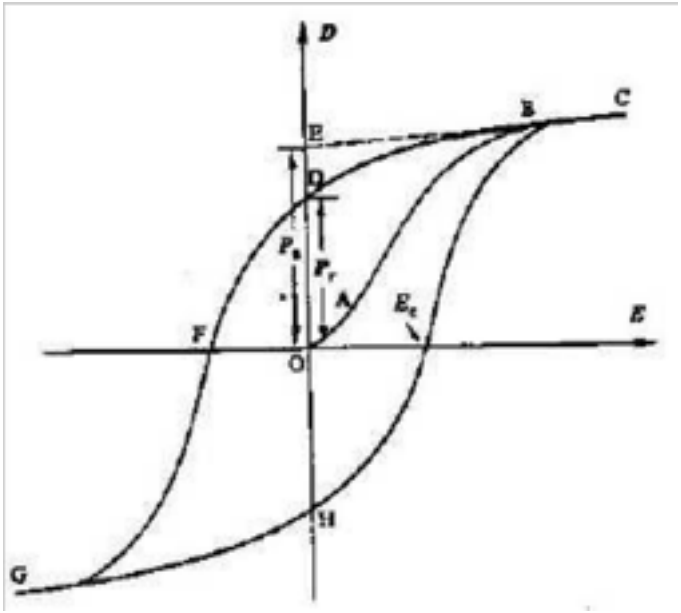

Figure 1.4: P-E Hysteresis loop.

In literature, only the outer P-E loop is typically shown. However, interior curves can be inscribed when we alter the field in a different sequence. For instance, if we start at a point of zero polarization and electric field, increase the field to a small amount (much less than

the coercive field) and then reverse it, the P-E loop will be a small minor loop centered on P=0,~E=0. In this way, the entire area of the P-E loop can be accessed by different sequences of applied electric field [17].

1.5 BNT

Between all the lead free ceramics (Bi, Na) TiO_3 based ceramics are considered to be good candidates because of it strong ferroelectricity. At room temperature, BNT has high Curie temperature (T_c=320 ˚C), a large remanent polarization (Pr =38 μC/cm^2) and coercive field (E_c =73 kv/cm) [18]. BNT perovskite shows high dielectric constant approximately 290-540 at low temperatures [19]. The material was studied continually by several researchers. In this system, two phase transformation was observed, which were cubic to tetragonal phase and tetragonal to rhombohedral phase. The transition from tetragonal to rhombohedral corresponds to a transformation from an antiferroelectric state to ferroelectric.

1.5.1 Crystal Structure and Phase Transition of BNT

Recently, Bismuth sodium Titanate (BNT) has attained significant attention from various scientists due to its very high field-induced electromechanical strain. This material has complex perovskite structure with chemical formula $Bi_{0.5}Na_{0.5}TiO_3$ as presented in Fig. 1.5. In the structure of BNT, half of all A-site positions are filled with bismuth (3+) ions, and the other half with sodium ions (1+) and the B-site positions are filled by titanium (4+) ions. This perovskite structure can be considered in two ways: one is to have the bismuth and sodium cation occupy the corners of cubic unit cell, oxygen cations occupy the face centers, and titanium cation is in the center of oxygen octahedra that was formed. The second way, is a three-dimensional cubic network of 8 corner-sharing TiO_6 octahedra with bismuth and sodium cations at the center of the cube formed by the octahedra. The fig.1.5 shows that the bismuth and sodium ions is ordered on the A-site of the structure.

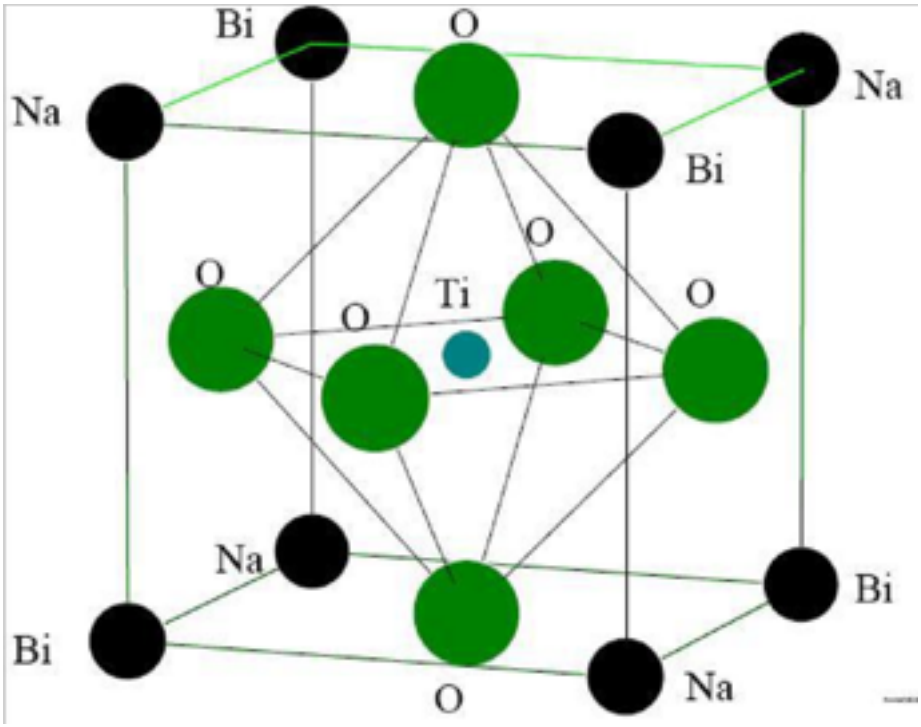

Figure 1.5: Representation of an ABO_3 perovskite structure shown as cubic BNT.

Many structural investigations have been performed on BNT since after its discovery. There are several reports conducted to determine the phases and phase transitions in BNT. In 2000, John and Thomas studied the phase transitions and crystal structure of BNT, at various temperatures [20]. The results (Table 1.1) showed that with decreasing temperature, BNT shows transformation from cubic to tetragonal and then to rhombohedral [21]. BNT is polar in rhombohedral phase due to the cation displacement, which allows the crystal to have a spontaneous polarization for a material to be ferroelectric. The tetragonal phase has weaker polarization response than the rhombohedral phase, it also has a polar phase. At room temperature and ambient pressure, BNT behaves like relaxor ferroelectric in the rhombohedral phase and it shows diffuse transformation between each of the phases. The evident in the dielectric response of BNT were diffuse phase transitions because the relative permittivity peaks become broad instead of having a sharp peak, like those seen in materials with Curie Weiss behavior [22-23].

Table 1.1: Phase transition in BNT.

Temperature (˚C)	-268 to 255	255 to 400	400 to 500	500 to 540	Above 540
Phase	Rhombohedral –R3c	Rhombohedral / Tetragonal	Tetragonal-P4bm	Tetragonal / Cubic	Cubic prototype-Pm3m
Lattice parameter (Å)	a_H = 5.4887 c_H = 13.5048	Variable	a_T =5.5179 c_T =3.9073	Variable	a_c =3.91368

CHAPTER 2: LITERATURE SURVEY

2.1 Literature review

In the present chapter, research work carried out on bismuth sodium Titanate (BNT) have been summarized.

BNT composition shows significant merit, when they are doped with foreign ions. Its dielectric and piezoelectric properties change, depending on the site occupied by the foreign ion in ABO_3 perovskite structure.

Table 2.1: List of common ion substitution in BNT with their different properties.

Content	**Valency**	**ε_r**	**D_{33} (pm/V)**	**tanδ**	**T_c (°c)**	**T_d (°c)**	**P_r (μC/cm)**	**E_c (kv/cm)**	**k_t (%)**
Ba[25]	2+	1600	120	<0.05	250	-	-	-	-
Ce[28]	3+	468.35	-	0.0499	-	-	-	-	-
Li [30]	1+	539.40	57.3	0.029	-	-	23.9	124	-
Mn[31]	4+	349.58	90	0.0182	-	-	381	34	44
Nb[32]	5+	487.48	-	0.0416	-	-	41.5	4.5	-
Y [33]	3+	-	1347	-	-	-	-	-	0.3
La [27]	3+	580.69	112	0.0408	269	-	-	-	-
Gd [29]	2+	577	-	0.038	341	108	25.92	28.92	-

Nagata et al., 2004 represented that with a sintering time of two hours the relative density of BNT shows a nearly linear increase with temperature from 90% at 1150°C to 98% at 1225°C. The samples were partially melted at temperature above 1225°C. At temperature 1100°C, sintering at two hours resulted in 87% relative density, which can be improved to

96% relative density after long time sintering. Instead from the standard mixed oxide route, sol gel method has been successfully applied to BNT [24].

Chaouchi et al., 2011 examined that $Bi_{0.5}$ $Na_{0.5}$ TiO_3 powders with doping of $BaTiO_3$ by sol gel method using acetate, nitrates and alkoxide as reactants. With thermal treatment performed at 800°C for two hours in air single phased powder were obtained. This result informs that $0.93Na_{0.5}Bi_{0.5}TiO_3$ -$0.07BaTiO_3$ ceramic contain good polarization behavior, with good dielectric, ferroelectric and piezoelectric properties at room temperature (ε_r = 1600, tanδ<0.05, T_c =250°C and d_{33} = 120pC/N) [25].

Cernea et al., 2010 examined the ceramics BNT-$BT_{0.08}$ prepared by sol gel technique, sintered at temperature 1100°C and 1150°C shows high mechanical quality factor (Q_m ~ 500) and good dielectric properties [26].

Pengpat et al., 2006 examined the (1-y) $(Bi_{0.5}$ $Na_{0.5})$ $_{(1-1.5x)}$ La_xTiO_3 (BNLT)-y$BaTiO_3$ (BT) powder ceramic where x=0.0172 and y = 0-0.2 by solid solution method and were sintered at 1150°C for all values of y. MPB phase was found at y = 0, also the maximum value of ε_r was obtained at room temperature. The maximum value of d_{33} and relatively low value of ε_r was obtained at y=1.5. In this ceramic, over wide range of temperature the very broad peak of ε_r with low dielectric constant was obtained which is useful in ultrasonic applications [27].

Razak et al., 2016 examined the ceramics BNCT and BNT by using soft combustion method. BNCT contain the lowest tanδ (0.0499) and the highest ε_r (468.35) in the presence of NBT, high density (5.588 g cm^{-3}) and small grain size (~421nm) [28].

Pal et al., 2014 examined the ceramic BNT with the doping of rare earth metal (Gd) with compositions x < 0.04, by a novel semi- wet technique, shows single phase formation with a rhombohedral structure at room temperature. Decrease in the size of grain with x shows that Gd acts as a grain growth inhibitor. For composition x= 0.02 transition temperature found to be maximum 'T_m' and 'Td' decreases continuously with x. x = 0.02 has shown

optimum piezoelectric and ferroelectric properties with low value of tanδ and minimum value of coercive filed 'E_c' [29].

AHN et al., 2013 examined the BNT-BT thin films with doping of Li by a metal deposition process. It was found that this ceramic significantly improves the piezoelectric and ferroelectric properties of BNT-BT thin films. The value of piezoelectric d_{33} and remanent polarization P_r increases with increase in Li content, showing maximum values at x=10, and then starts decreasing with increase in Li component. In BNT-BT Li10 films shows a high P_r of 23.9 μC/cm^2 under an applied electric field of 124kv/cm and local effective piezoelectric d_{33} 57.3pm/V [30].

Wang et al., 2014 examined the BNT-BT ceramic with the doping of 0.5 mol% of Mn, by solid solution method, enhances the electrochemical property, piezoelectric, structural thermal stability and reduces the development of tetragonal phase as temperature reaches T_m upon heating. The composition BNT-0.5Mn and BN7.5BT0.5Mn contain higher Td and d_{33} than BNT and BN7.5BT respectively. The d_{33} values for BNT, BNT-0.5Mn, BN7.5BT and BN7.5BT-0.5Mn comes out to be 79, 90, 185 and 190 pC/N respectively. The values of electrochemical factor (k_t) for BNT, BNT-0.5Mn, BN7.5BT and BN7.5BT-0.5Mn are about 40%, 44%, 46%, and 47 % respectively. The values of P_r and E_c for BNT, BNT-0.5Mn, BN7.5BT and BN7.5BT-0.5Mn are about 32lC/cm^2 and 40 kV/cm, 38lC/cm^2 and 34kV/cm, 42lC/cm^2 and 22kV/cm, 40lC/cm^2 and 24kV/cm [31].

Zuo et al., 2009 examined the BNT ceramic with the small amount of doping of Nb^{5+} ceramics were synthesized by solid state reaction method. With the doping of Nb^{5+} up to 3 mol% the average grain size of BNT is reduced. Improvement in ferroelectric and electrical properties and electrochemical factor was found due to the increase in resistivity and enhanced densification due to the formation of A-site vacancies. With 1% mol Nb^{5+} doping in BNT contains a P_r of 41.5 μC/cm and E_c of 4.5 kv/mm. The values of P_r is increased and E_c is decreased by doping of Nb^{5+} compared to pure BNT [32].

Zhou et al., 2009 examined the effects of Y_2O_3 on BNT by conventional solid state method. Their result showed, a decrease in average grain size with increase in Y_2O_3. With the doping

amount of 0.5%, Y_2O_3 revealed the improvement in the piezoelectric coefficient d_{33} by a value 137 pC/N and electrochemical coupling factor k_p with the value of 0.3 [33].

K.N Singh et al., 2015 examined the effect of Antimony doped on pure BNT ceramics by using a conventional solid state reaction route. At 0.03% Sb doped with the BNT, Xray diffraction analysis showed a probable structure change. At around x=0.03 Morphotropic phase boundary (MPB) may exist [34].

Eaksuwanchai et al., 2014 examined the effect of $Sr_{0.92}La_{0.08}TiO_3$ on $Bi_{0.5}$ $Na_{0.5}$ TiO_3 ceramics by using a conventional solid state reaction method. The sintering is done at temperature 1500°C for 3h. X-ray diffraction analysis showed that all ceramic compositions contain a cubic structure with slight lattice contraction with BNT addition [35].

Kang et al., 2015 examined the BNT-BT ceramic with composition of 0.2, 0.4, 0.6, 0.8, and 0.10 by a mixed oxide method. By using xrd analysis the ABO_3 perovskite structure is confirmed. Due to the existence of phase transition, the value of relative dielectric permittivity is increased with increasing BT content. P-E hysteresis loop shows that

BNT-BT ceramic contain strong ferroelectric properties as the BT content increased [36].

Glaum et al., 2013 examined the effect of Zr on BNT-BT ceramic results in the appearance of stable Ti-O dipoles, thus stabilizing the electrically induced preferred domain orientation. For low Zr levels the degree of disorder is not changed significantly, which leaves the transition temperature T_{F-R} unchanged. For higher Zr levels, the stabilizing effect becomes zero, the transition between the relaxor and ferroelectric state becomes reversible close to room temperature [37].

Acosta et al., 2012 examined the ceramics in two composition, BNT–BT–CZ and BNT–BT–KNN–CZ were successfully synthesized by using mixed oxide route and their electrical, dielectric and structural properties were investigated. Temperature operational windows of at least 400°C with less than 15% variation in their ε_r and average values from

~470 up to ~2300 were observed. At 300°C the dielectric loss factor lies below ~10% and RC constant ranging from ~0.03s up to ~4s [38].

Tian et al., 2012 examined the structural, ferroelectric and magnetic properties of BNTBF with composition of 0 to 0.6 by solid solution method. At room temperature for x = 0.3 enhanced multiferroic properties with remanent polarization P_r = 1.49 μC/cm^2 and saturated magnetization M_s= 0.51 emu/g. Also the transition from PM to FM is observed, this transition can be attributed to the existence of long range superexchange of Fe^{3+}-O-Ti-O-Fe^{3+} in the chemically ordered regions [39].

Yuan et al., 2010 examined the effect of $CaTiO_3$ on BNT-BT at high temperature capacitor by using conventional oxide method. The doping of CT increases the dielectric constant at low temperature where decreases the dielectric constant at high temperature, so that the variation of capacitance decreases. With the addition of dopants BT and CT, a single- phase perovskite structure and square grains were observed. If the proper amount of BT and CT were added, the temperature characteristic of capacitance in temperature range from -55°C to 200°C was within ±15% [40].

Nguyen et al., 2012 examined the effect of co-doping with Ta and Li ions on BNKT ceramic by solid solution method, and their microstructure, crystal structure, ferroelectric, and EFIS properties were investigated. It was observed that Li-doping on A-sites also results in a FE-NP phase transition, on other side the B-site doping results in a large strain near the phase boundary. Also Li doping shows a diffuse FE-NP phase transition than Ta doping [41].

Ehmke et al., 2011 examined the ceramic 0.94BNT-0.06BT with or without doping of 1%mol CuO under bipolar loading. The doping of 1% mol of CuO was observed to successfully suppress the electric fatigue without changing the electrochemical properties (polarization and strain). In BNBT0Cu ceramic, the electric field induced symmetry will change from rhombohedral to tetragonal, where in BNBT1Cu the tetragonal phase is stabilized by addition of CuO so it does not undergo these transition [42].

Selvamani et al., 2012 examined the ceramic (1-x) NBT-x$BiCrO_3$ by solid solution and measurements of ac conductivity. These measurement shows that with increase in $BiCrO_3$ content the electrical conductivity and dielectrical loss of NBT also increases. The impedance measurements shows that the conductivity of 0.85NBT-0.15$BiCrO_3$ is higher than pure NBT [43].

2.2 Objectives

1. To prepare BNT and BNBT (Ba doped BNT) ceramics by using auto combustion method.

2. To study the effect of Ba doping on the structural, dielectric and ferroelectric properties of BNT.

CHAPTER 3: EXPERIMENTAL DETAILS

3.1 Sol-gel autocombustion method

The sol-gel process is a wet chemical technique used in the field of material science. Such methods are used for the preparation of materials (typically metal oxides) starts from the colloidal solution that perform as the precursor for an integrated network (or gel) of either discrete particles or network polymers. Precursors are typically metal alkoxides and metal salts (such as chlorides, nitrates and acetates), which undergoes different forms of hydrolysis and polycondensation reactions. Glycine is used as fuel for combustion to take place. The heat of combustion of glycine (-3.24 Kcal/g) is much higher as compared to other organic fuels such as urea (-2.98 Kcal/g) and citric acid (-

2.76 Kcal/g).

3.2 Preparation of Bismuth Sodium Titanate (BNT)

Bismuth Sodium Titanate (BNT) powder was prepared by Sol-gel combustion method. The raw materials used for the experiment were bismuth nitrate pentahydrate [Bi $(NO_3)_3.5H_2O$] with 98% purity, sodium nitrate [$NaNO_3$] with 99% purity, Titanium (IV) isopropoxide [$C_{12}H_{28}O_4Ti$] with purity 97%, glycine [H_2NCH_2COOH], nitric acid and distilled water. The procedure for preparation is as follows:

Firstly, bismuth nitrate pentahydrate was dissolved at room temperature in the nitric acid and distilled water mixture for hour. When the solution became transparent, sodium nitrate was added to it. As the solution became transparent titanium isopropoxide was mixed by constant stirring at room temperature for another one hour. The resultant solution was transparent and clear. The glycine was dissolved in the solution. The solution was heated at 80 °C with constant stirring for 4 hrs, till there was an immense evolution of light brown fumes, towards the end of reaction a fluffy yellow mass (gel) was obtained at the base of

beaker which got converted into powder. The powder so obtained was kept in hot air oven at 110 °C for overnight. The powder was then ground in agate mortar for 2 hrs. The so obtained powder was calcined at 750 °C with for 10 hrs in a tubular furnace with heating and cooling rate maintained at 5 °C per minute. Fig.

3.1 shows the flow diagram of the preparation of BNT powder.

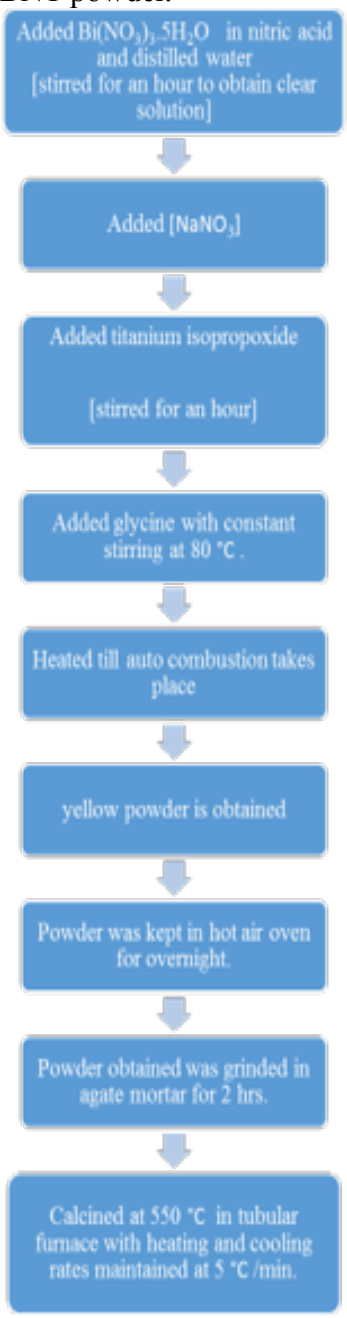

Figure 3.1: Flow chart for BNT powder preparation.

3.3 Preparation of Ba doped BNT

Similar method was obtained to prepare Ba doped BNT. The raw materials used for the experiment were bismuth nitrate pentahydrate [Bi $(NO_3)_3.5H_2O$] with 98% purity, sodium nitrate [$NaNO_3$] with 99% purity, Titanium (IV) isopropoxide [$C_{12}H_{28}O_4Ti$] with purity 97%, barium nitrate Ba (NO_3) purity 99%, glycine [H_2NCH_2COOH], nitric acid and distilled water.

This powder was used make pellets. The samples were sintered at 780°C for 10 hours in the tubular furnace with heating and cooling rate maintained at 5°C per minute. The pellets were polished using silver paint was applied as electrodes used for dielectric, P-E hysteresis loop and piezoelectric measurements. The flow chart for preparation Ba doped BNT is given below in figure 3.2.

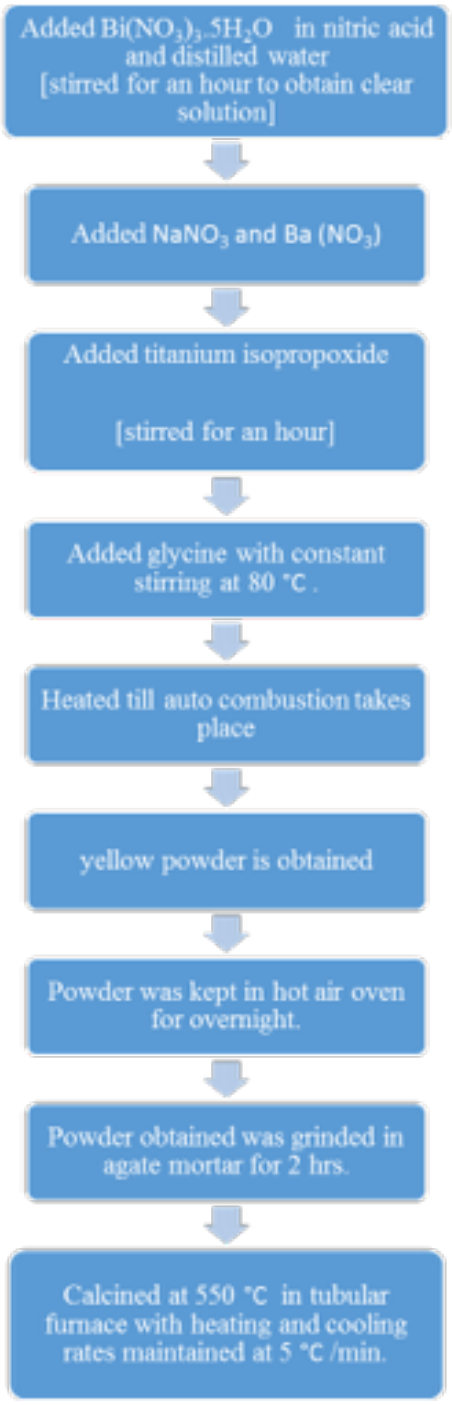

Figure 3.2: Flow chart for BNBT powder preparation.

3.4 Characterization Techniques

The characterization techniques which were used for analysis of samples are given below:

3.4.1 X-Ray Diffraction (XRD)

X-ray diffraction is a technique used for identification of phase of a crystalline material and it also provides information on unit cell dimensions. Xrd techniques are a family of non-destructive techniques which gives information about the crystal structure, chemical composition, and physical properties of material. The image of XRD machine is given in fig 3.3.

Figure 3.3: XRD machine.

Bragg's law:

Bragg diffraction occurs when radiation of wavelength comparable to atomic spacings, is scattered in a specular fashion by the atoms of a crystalline system, and undergoes constructive interference. The waves are scattered from lattice planes separated by the interplanar distance d for a crystalline solid. When the scattered waves interfere constructively, they remain in phase since the difference of the path lengths of the two waves is equal to an integer multiple of the wavelength. The path difference between the two waves undergoing interference is given by $2d\sin\theta$, where θ is the scattering angle. The effect of the destructive or constructive interference intensifies because of the cumulative effect of reflection in successive crystallographic planes of the crystalline lattice. This

results in Bragg's law, which shows the condition on θ for the constructive interference to be at its strongest. Fig 3.4 shows the diagram of Bragg's law.

$$2d\sin\theta=n\lambda$$

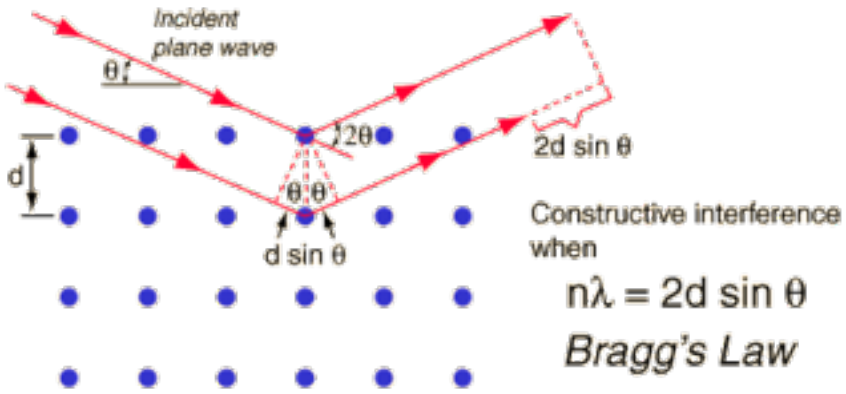

Figure 3.4: Bragg's law

Where n is a positive integer and λ represents the wavelength of incident wave. Note that moving particles, have an associated wavelength known as de Broglie wavelength. A diffraction pattern is acquired by measuring the intensity of scattered waves as a function of scattering angle. Strong intensities known as Bragg peaks are acquired in the diffraction pattern at the points where the scattering angles satisfies the Bragg condition.

3.4.1.1 Essential parts of Diffractometer

- X-Ray Tube: the source of x-rays.
- Incident beam optics: condition the x-ray beam before it hits the sample.
- The goniometer: the platform that holds and moves the sample, detector.
- The sample and sample holder.

- Receiving side optics: condition the x-ray beam after it has encountered with the sample.
- Detector: count the number of x-rays scattered by the sample.

3.4.1.2 Advantages of XRD

- Rapid and powerful technique for identification of an unknown material.
- In this technique, minimum sample preparation is required.
- Data interpretation is straight forward.
- XRD units are widely available.

3.4.1.3 Applications of XRD

- It is a non-destructive technique.
- To identify crystalline phases and orientation.
- To measure thickness of thin films and multi-layers.
- To determine atomic arrangement.
- To determine structural properties: strain, grain size, phase composition, epitaxy etc.

3.4.2 LCR Meter

An LCR meter is an electronic test device used to measure inductance (L), capacitance (C) and resistance (R) of an electronic component. The image of the LCR meter is given in fig 3.5.

Figure 3.5: LCR Meter.

3.4.2.1 Types of LCR meters

There are two types of LCR meters- benchtop and handheld.

- Benchtop

  These are developed for bench applications and are kept at fixed location without any movement. Benchtop LCR meters have selectable test frequencies of more than 100 kHz.

- Handheld

  These are developed for portable applications .These can be moved around for test and measurement purpose. Handheld LCR meters have selectable test frequencies of 100 Hz, 120 Hz, 1 kHz, 10 kHz and 100 kHz for top end meters.

3.4.2.2 Advantages of LCR meter

The advantages of LCR meter are given below:

- It is friendly to operate.
- It measures passive components with minimum errors.
- This instrument is very easy on calibration.
- There are many manufacturers of LCR meter hence more features and options are available for user to purchase.

3.4.3 Ferroelectric Hysteresis Measurement

Hysteresis is a phenomenon that is present in all piezoelectric materials and the existence of a hysteresis loop (P-E) has been considered as evidence towards establishing that a material is ferroelectric. Hysteretic behavior is due to the lossy nature of the ceramic where the current trails the applied voltage by an angle related to the loss tangent of the material. The polarization P is a double – valued function of the externally applied electric field E. If a small electric field is first applied, only a linear relationship between P and E exists because domains stay in their initial configuration. As the electric field strength increases, the domains, whose polarization direction is opposite to the field will be switched. Consequently, the polarization increases significantly with increasing E until all of the domains are aligned in their field direction. This state is called the state of saturation.

Theoretically, this state of saturation polarization should correspond to a single domain state of the crystal. When the field is zero, the polarization does not return back to zero. Rather, the domains remain aligned, and crystal exhibit a remnant polarization P_r. The strength of the field necessary to reduce the polarization to zero is called coercive field E_c. Further increase of the field in the opposite direction will cause a complete alignment of the dipole domains in this opposite direction. Finally, by reversing the field once again, the process can be repeated. To characterize the amount of hysteresis in a ceramic, a sinusoidal voltage is applied to the device and the displacement is recorded.

By plotting the displacement vs. driving voltage the hysteretic behavior of the ceramic can be observed.

Experimentally, ferroelectric hysteresis loops can be measured using a Sawyer – Tower circuit or a modified version of it, applying an a.c. field and can be observed on the screen of an oscilloscope. The circuit is shown schematically in figure 3.6.

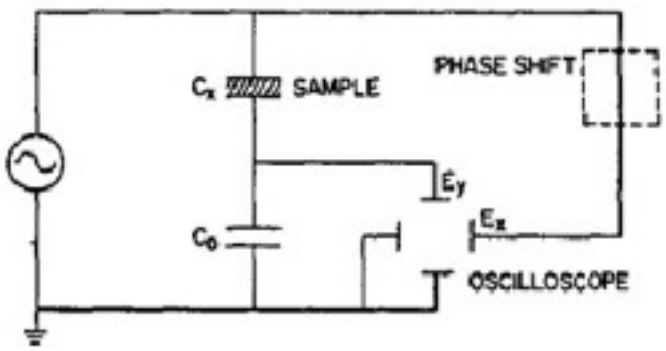

Figure 3.6: Modified Sawyer-Tower Circuits

Horizontal axis uses the voltage across the sample and a quantity which is proportional to the field across the sample is plotted on this axis. The resulting charge stored on the sample is determined by means of a large reference capacitor C_o placed in series with the sample. In this configuration, the voltage across C_o is proportional to the polarization of the sample. An electrometer can be used to detect the voltage across the capacitor; by multiplying this voltage with the value of the reference capacitor, the charge across the sample results. The reference capacitor should be 100 to 1000 times the value of the capacitance of the sample. This polarization is laid across the vertical plates of the oscilloscope. This circuit not only measures the hysteresis but also quantifies the spontaneous polarization (P_s) and coercive field (E_c).

3.4.4 Scanning Electron Microscope

In scanning electron microscopy (SEM) an electron beam is focused into a small probe and is rastered across the surface of a specimen. Several interactions with the sample that result in the emission of electrons or photons occur as the electrons penetrate the surface. These emitted particles can be collected with the appropriate detector to yield valuable information about the material. The most immediate result of observation in the scanning electron microscope is that it displays the shape of the sample. The resolution is determined by beam diameter. The image of the SEM instrument in given in fig 3.6.

Figure 3.6: SEM Instrument

In scanning electron microscopy visual inspection of the surface of a material utilizes signals of two types, secondary and backscattered electrons. Secondary and backscattered electrons are constantly being produced from the surface of the specimen while under the electron beam however they are a result of two separate types of interaction. Secondary electrons are a result of the inelastic collision and scattering of incident electrons with specimen electrons.

CHAPTER 4: RESULTS AND DISCUSSION

In the proposed work, the synthesis of BNT with the doping of Ba is done by using sol gel autocombustion method, the samples were then calcined at 750°C with holding time of 10 hours. Four samples were prepared by varying the concentration of barium content.

Table 4.1 shows the initial ingredients for the preparation of sample.

Table 4.1: Initial ingredients.

Sample Name	**Amount of chemicals used (in gm)**			
	Bismuth nitrate [$Bi(NO_3)_3.5H_2O$]	**Sodium nitrate [$NaNO_3$]**	**Barium Nitrate $Ba(NO_3)$**	**Titanium isopropoxide [$C_{12}H_{28}O_4Ti$]**
BNT 0	6.06337	1.06237	0	7.1054
BNT 0.02	5.9421	1.0411	0.1307	7.1054
BNT 0.04	5.8208	1.0199	0.2613	7.1054
BNT 0.06	5.6996	0.9986	0.3920	7.1054

4.1 X-ray diffraction results:

The XRD results revealed the different phases formed in the samples. The results were studied by matching them with various standard ICDD cards, which gave information about the constituent phases present in the samples. The matching was done with the

X'pert Highscore Plus tool. All the four samples contained the peaks of BNT. Below fig 4.1 shows the XRD pattern of BNBT ceramic.

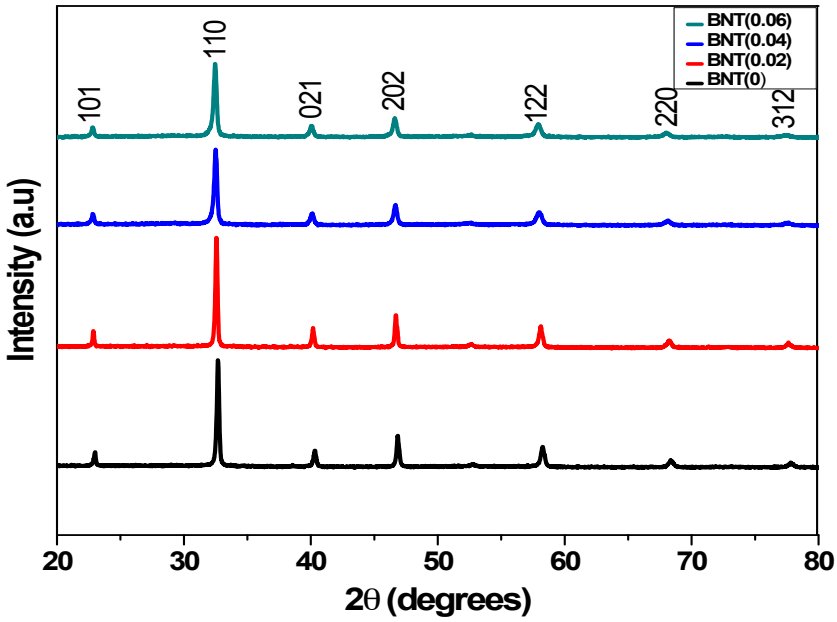

Figure 4.1: XRD pattern of samples. (a) BNB_xT (x=0). (b) BNB_xT (x=0.02). (c) BNB_xT (x=0.04). (d) BNB_xT (x=0.06).

Fig 4.1 (a-d) shows the XRD pattern of BNB_xT (x=0, 0.02, 0.04 and 0.06). There are seven diffraction peaks observed for the BNT phase for the planes (101), (110), (021), (202), (122), (220) and (312) (ICDD Card No.00-036-0340) in every synthesized sample. These peaks belong to rhombohedral structure with space group Pm-3m. The Diffraction pattern revealed that all the samples show single phase formation with rhombohedral structure and no peaks of secondary phases were observed. It implies that Ba^{2+} ions have diffused into the Bi^{3+} site and homogeneous solid solution is formed. The calculated lattice parameters for samples are tabulated in table 4.2. The lattice parameter are found to be increased with increase in Ba content. It implies that the Ba (1.61 A°) ions with larger ionic radii have diffused into the BNT lattice and resulted in the enlargement of lattice. The formula to calculate lattice parameter for rhombohedral structure is given below.

$$\frac{1}{d^2} = \frac{(h^2+k^2+l^2)\sin^2\alpha + 2(hk+kl+hl)(\cos^2\alpha-\cos\alpha)}{a^2(1-3\cos^2\alpha+2\cos^3\alpha)} \qquad (4.1)$$

It was observed from the Fig. 4.2 that the substitution of barium in BNT shifts the peak position towards lower angle side. It was investigated from the previous work that on further increase in the barium concentration in BNT leads to a change in the structure of the materials from rhombohedral to tetragonal structure. In present work it was observed that on increasing barium content (up to x = 0.06) in BNT the crystal structure of the material remains same.

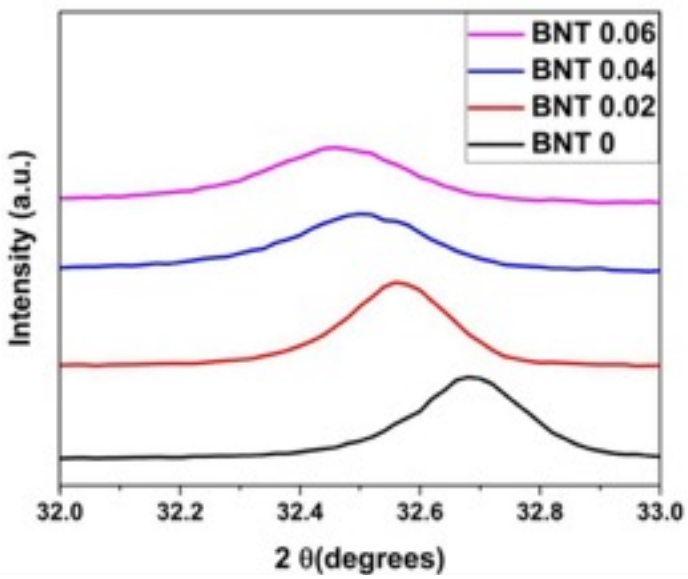

Figure. 4.2: Zoomed in view of x ray diffraction of BNB_xT (x= 0, 0.02, 0.04, and 0.06) at 2θ= 32-33°

Figure 4.2 shows the enlarged view of BNBT peaks. The Debye Scherer equation was used to calculate the average crystallite size of all the samples, which is given in equation (4.2)

$$t = k\lambda/\beta_{size}\cos\theta \qquad (4.2)$$

Where t = average crystallite size,

β_{size} = line broadening in radians, θ =

Bragg angle, λ = X ray wavelength, k

= Scherer constant.

Table 4.2: Physical properties of all the samples of BNBT.

Compositions (x)	**Lattice Parameter (Å)**		**Volume (Å)^3**	**Average Crystallite Size (nm)**	**Strain ε (%)**
	a=b	**c**			
BNB_xT (0)	5.479	6.867	176.02	54.96	0.0023
BNB_xT(0.02)	5.504	6.871	176.02	43.94	0.0029
BNB_xT(0.04)	5.707	6.887	176.02	39.93	0.0032
BNB_xT(0.06)	5.777	6.911	176.02	33.80	0.0038

The strain was calculated from the formula:

$$\beta = \beta_{size} + \beta_{strain}$$

where, $\beta_{size} = k\lambda/t\cos\theta$,

and $\beta_{strain} = 4\eta\tan\theta$

$$\beta = (k\lambda/t\cos\theta) + 4\eta \tan\theta$$

$$\beta \cos\theta = (k\lambda/t) + 4\eta \sin\theta$$

$$\beta \cos\theta/\lambda = (k/t) + T\sin\theta \qquad (4.3)$$

Where T is the strain in the system. Hence by plotting β cos (θ) vs 4 sin(θ) (shown in Fig. 4.3), we can find the crystallite size from the intercept of the line at x = 0 and the slope value estimates the strain, The calculated crystallite size and the strain are given in Table 4.2.

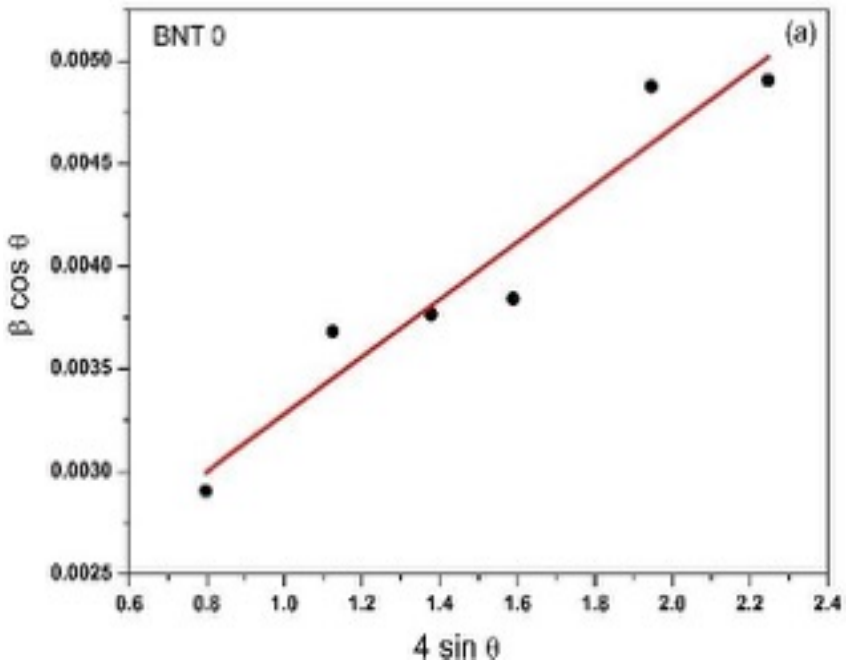

(a)

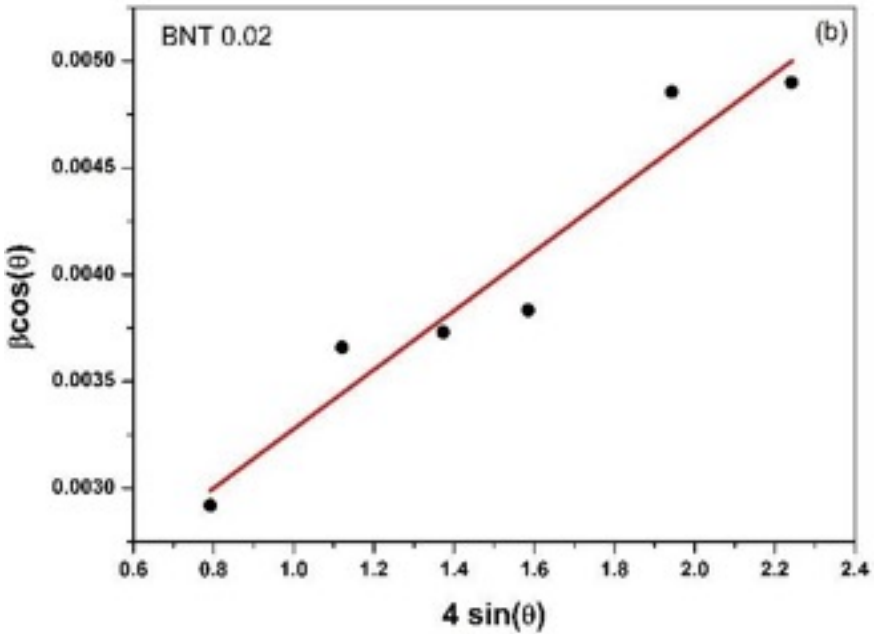
BNT 0.02
(b)
0.0050
0.0045
0.0040
0.0035
0.0030
βcos(θ)
0.6
0.8
1.0
1.2
1.4
1.6
1.8
2.0
2.2
2.4
4 sin(θ)

(b)

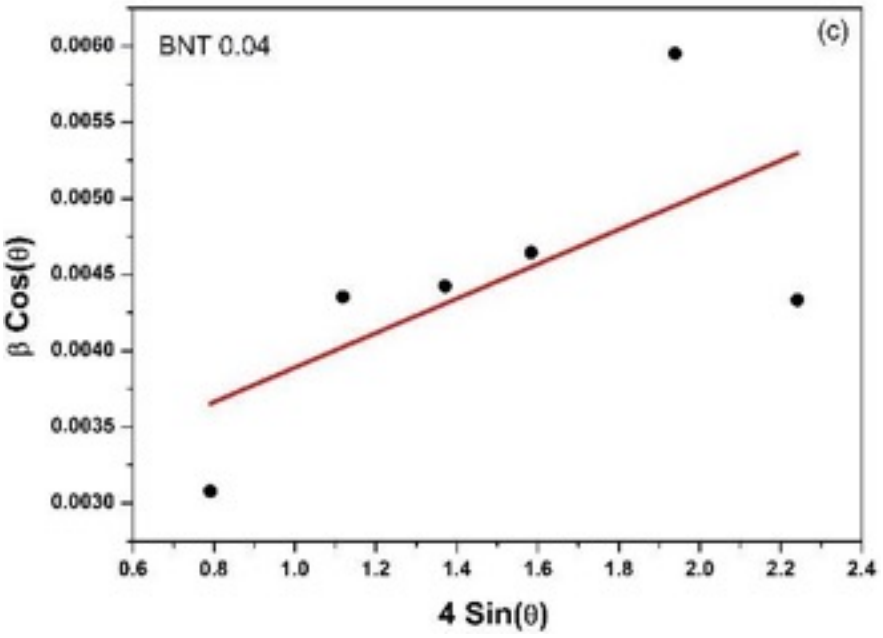
BNT 0.04
(c)
0.0060
0.0055
0.0050
0.0045
0.0040
0.0035
0.0030
β Cos(θ)
0.6
0.8
1.0
1.2
1.4
1.6
1.8
2.0
2.2
2.4
4 Sin(θ)

(c)

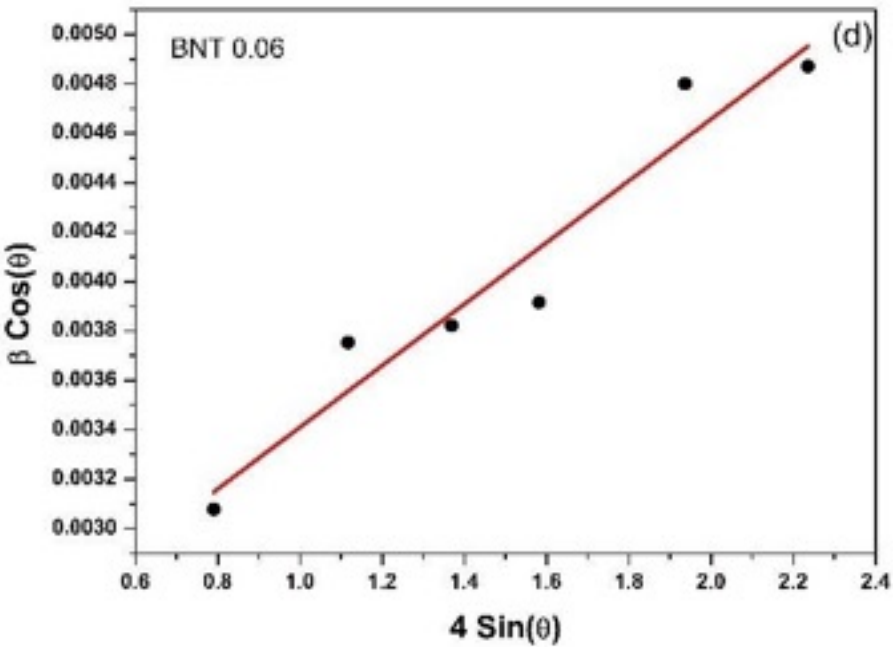

(d)

Figure. 4.3: The Variation of β cos (θ) vs 4 sin (θ) for BNB_xT ceramics (a) x = 0, (b) x = 0.02, (c) x =0.04, and (d) x = 0.06.

4.2 SEM

The microstructures of all the sintered samples of BNBT ceramics are shown in Fig. 4.4. The grain size of these ceramic samples decreases with increasing concentration of barium from (x = 0, 0.02, 0.04, and 0.06). Homogeneous distribution of grains is observed for all the samples.

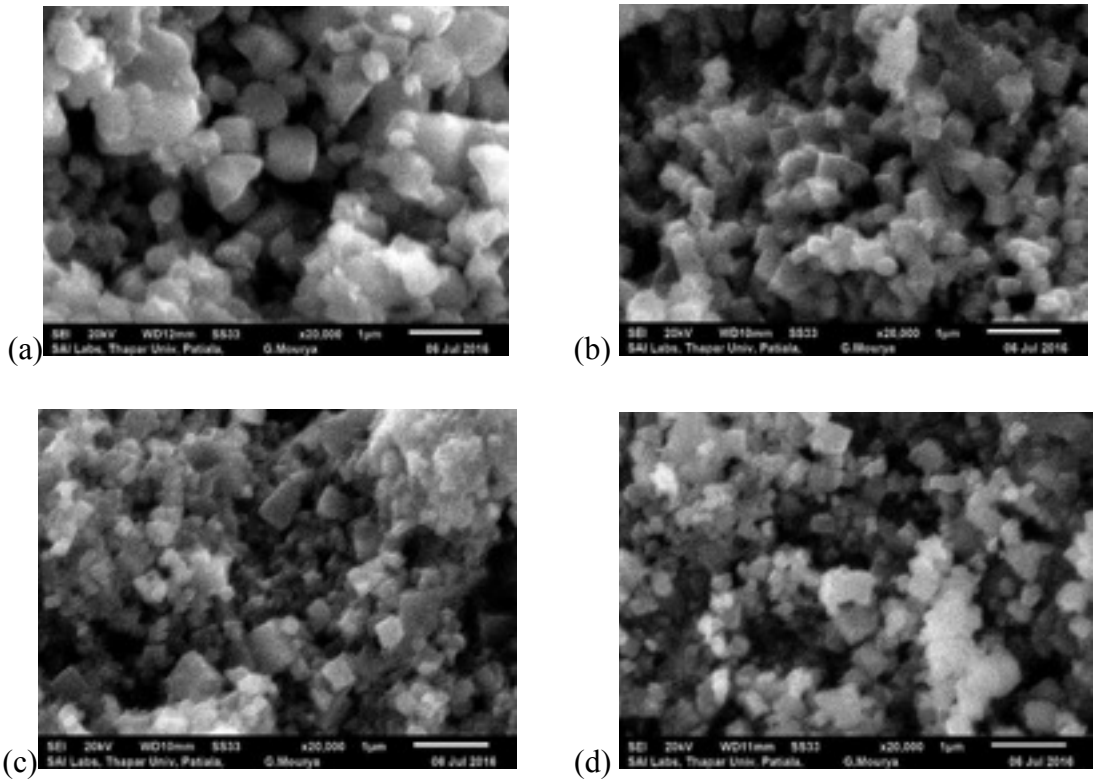

Figure 4.4: The microstructure of sample BNB_xT ceramics (a) x = 0, (b) x = 0.02 (c) x = 0.04 and (d) 0.06.

4.3 Dielectric

Fig 4.5 shows the variation of dielectric constant (ε_r) and dielectric loss (tan δ) with frequency at room temperature. Both are found to be decreased with increasing frequency, which is usual behavior of dielectrics. At low frequencies, dipoles follow the field but they began to lag behind the frequency at higher values.

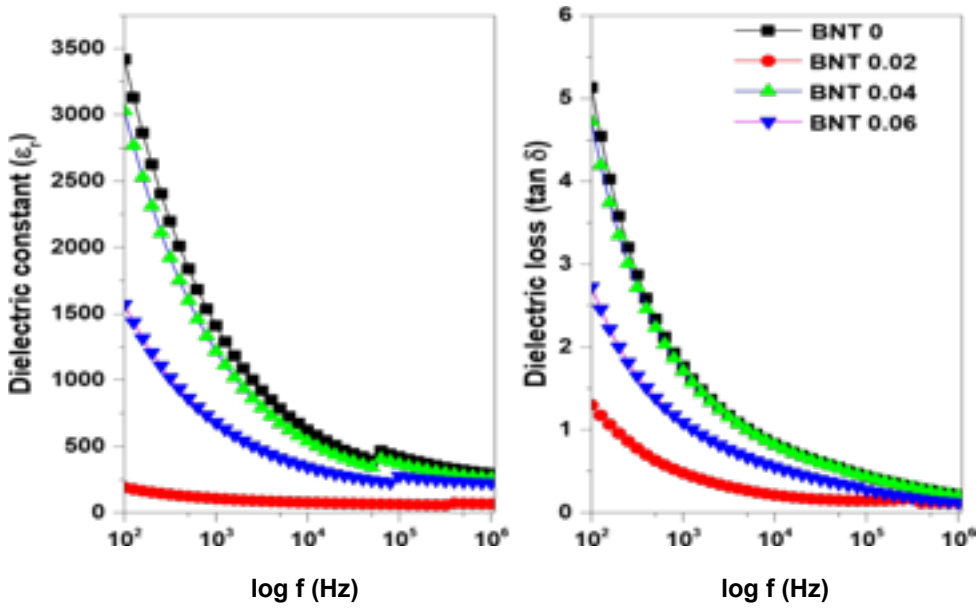

Figure 4.5: The variation of dielectric constant (ε_r) and dielectric loss (tanδ) with frequency of samples BNB_xT ceramics (x = 0, 0.02, 0.04 and 0.06).

The temperature dependence of dielectric loss and dielectric constant of all the synthesized samples of BNB_xT (x=0, 0.02, 0.04 and 0.06) at frequencies 100 Hz, 1 kHz, 10 kHz, and 100 kHz, 1 MHz f are shown in fig 4.6(a-d).

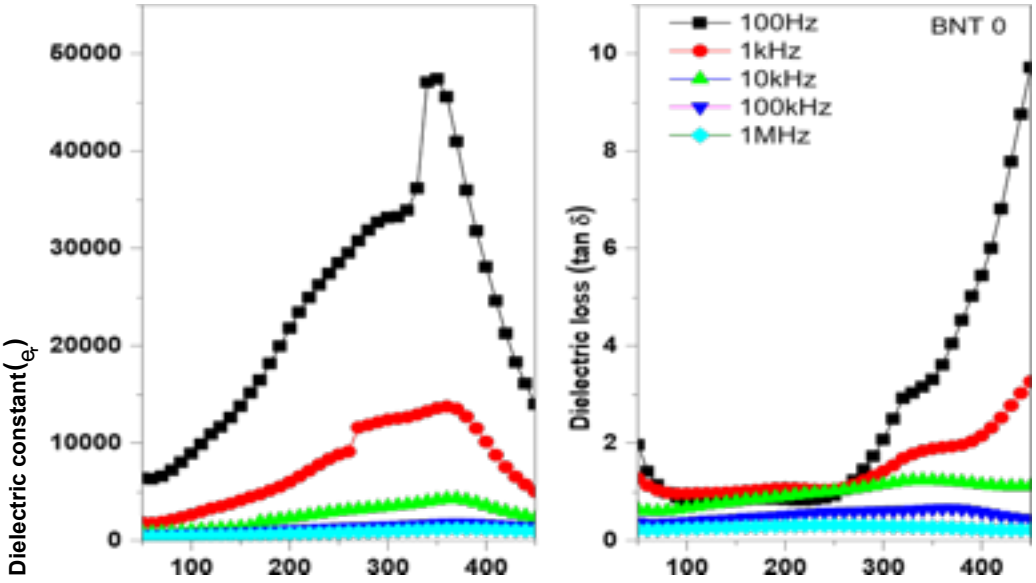

Temperature (°C) Temperature (°C)

(a)

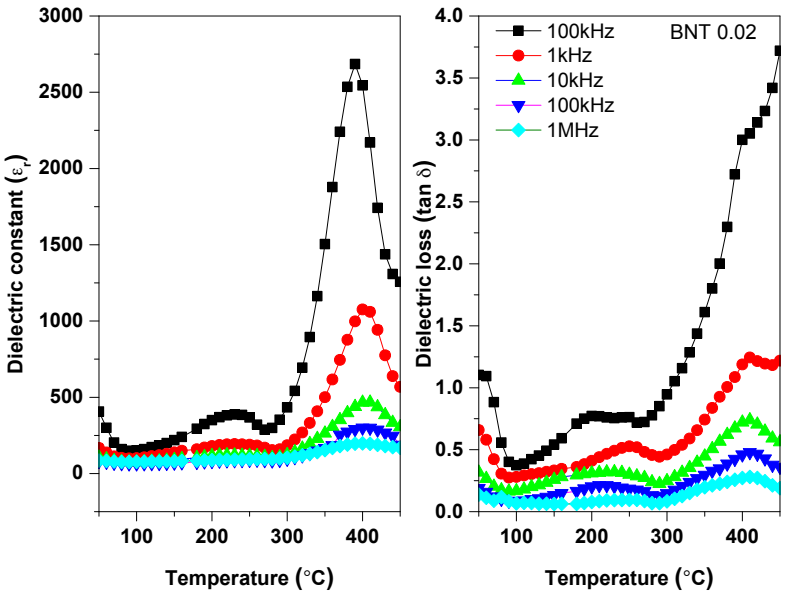

(b)

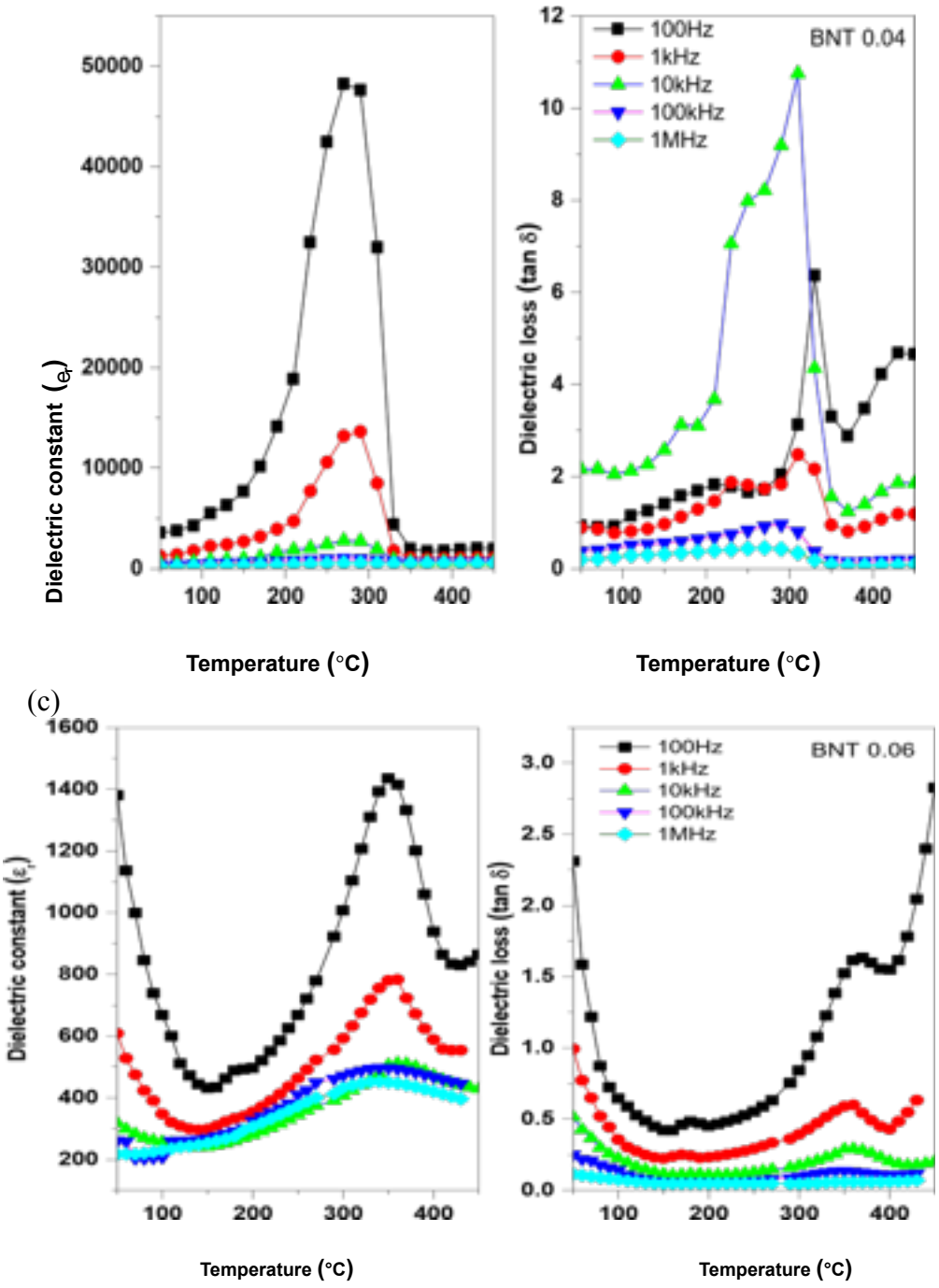

Figure 4.6: The variation of dielectric constant (ε_r) and dielectric loss (tanδ) with temperature of samples BNB_xT ceramics (a) x = 0, (b) x = 0.02 (c) x = 0.04 and (d) 0.06.

Fig 4.6 shows that dielectric constant is increased with temperature upto a certain temperature corresponding to (T_c = 320°C) and then it decreases with further increase in temperature. Similar anomaly is observed in dielectric loss. In BNT another anomaly corresponds to depolarization temperature T_d. In the synthesized BNT samples a very broad anomaly is evident because of the possible space charges due to volatile nature of Bi^{3+} ions. The dielectric constant is found to be decreased with increase in frequency from 100 Hz to 1 MHz. Because of diffused phase transition, all the samples show the typical character of a ferroelectric relaxor. Similar anomalies are observed for Ba doped samples as shown in fig 4.6 (a-d)

4.3 P-E Loop

The P-E loop of all the samples of BNBT ceramic are shown in the fig 4.7. The P–E loops obtained at room temperature become slightly broadened, Ec and Pr increase slightly, as the concentration of barium content increases. However, as concentration of barium is further increased from 0.02 to 0.04, the P_r decreases significantly and the E_c increases slightly as shown in fig 4.7.

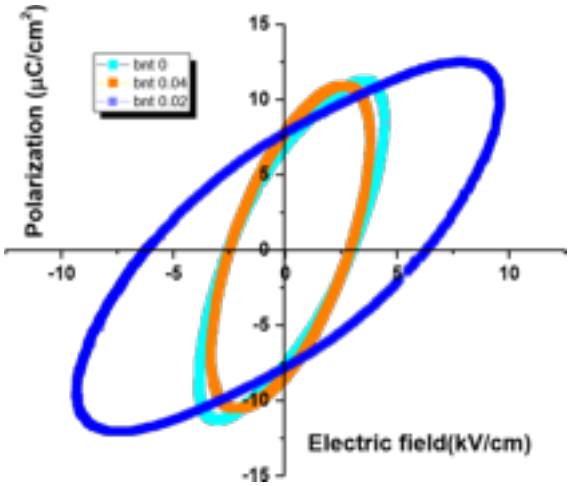

Figure 4.7: Room temperature P-E loop of all the samples of ceramic BNB_xT (x = 0, 0.02, 0.04 and 0.06).

CHAPTER 5: CONCLUSION AND FUTURE SCOPE

Phase pure BNBT powder can be prepared at a temperature as low as 750 °C by sol gel auto-combustion route, have shown single phase formation with a rhombohedral structure at room temperature. With the increase in the amount of dopant grain size, decreased considerably. This decrease in the grain size with Ba indicates that Ba acts as a grain growth inhibitor. However, the lattice parameters were found to be increased with increasing amount of x. With increase in frequency from 100 Hz to 1 MHz dielectric constant decreases. All the samples show the typical character of a ferroelectric relaxor.

Future Scope.

- To study the impedance analysis of the synthesized samples.
- To study the effect of sintering on the ferroelectric properties.

6. Reference

1. S. Cheong and M. Mostovoy, Nature Materials 6 (2007) 13-20.

2. Z.G. Ye, Material Research Society Bulletin 34 (2009) 277-282.

3. G.H. Haertling, Journal American Ceramic Society 82 (1999) 797–818.

4. B. Jaffe, W.R. Cook and H. Jaffe, Piezoelectric Ceramics, Academic Press, London (1971).

5. E. Cross, Nature 432 (2004) 24.

6. U.S. Department of Health and Human Services, Public Health Service, Agency for Toxic Substances and Disease Registry (2007).

7. G.A. Smolenskii, V.A. Isupv, A.I. Afranovskaya and N.N. Kainik, Journal of Solid State Physics 11 (1961) 2651.

8. P.Y. Goh, K.A. Razak and S. Sreekantan, Journal of Alloys and Compound 475 (2009) 758.

9. W.C. Lee, C.Y. Huang, L.K. Tsao and Y.C. Wu, Journal of the European Ceramic Society 29 (2009) 1443.

10. D. Damjanovic, The Science of Hysteresis, Elsevier Inc. (2005).

11. D. Damjanovic, Annales de Chimie Science des Materiaux, 26 (2001) 99-106.

12. S. Burianova, J.P. Vejpravova, P. Holec, J. Plocek and D. Niznansky, Journal of Applied Physics 110 (2011) 073902.

13. Z.M. Lei, W.C. Lei, Z. Wei, W.J. Feng and L.I. Zheng, State Key Laboratory of Crystal Materials and School of Physics and Microelectronics, Shandong University, Ji'nan, Vol. 20, (2003).

14. Bond valence structure analysis of doped Bismuth Sodium Titanate by Conor James Walsh, Alfed University, New York (2004).

15. P. Monod, J.J. Prejean and B. Tissier, Journal of Applied Physics 50 (1979) 7324.

16. A. Safari, R.K. Panda, and V.F. Janas Ferroelectric Ceramics: Processing, properties and applications 528 (2013) 22-*23*.

17. A. Manbachi and Cobbold, Ultrasound 19 (2011) 187–196.
18. R. Valenzuta, Magnetic Ceramics, Cambridge University press, New York (1994).

19. D.Z. Zhang, X.J. Zheng, X. Feng, T. Zhang, J. Sun, S.H. Dai, L.J. Gong, Y.Q. Gong, L. He, Z. Zhu, J. Huanga and X. Xu, Journal of Alloys and Compound 504 (2010) 129.

20. A. Franco, F.L.A. Machado and V.S. Zapf, Journal of Applied Physics 110 (2011) 053913.

21. I. Sharifi, H. Shokrollahi, M.M. Doroodmand and R. Safi, Journal of Magnetism and Magnetic Materials 324 (2012) 1854–1861.

22. I.P. Pronin, P.P. Syrnikov, V.A. Isupov, V.M. Egorov, N.V. Zaitseva and A.F. Ioffe, Ferroelectrics 25 (1980) 395.

23. J.V. Zvirgzds, P.P. Kapostis, and T.V. Kruzina, Ferroelectrics 40 (1980) 75.

24. H. Nagata, T. Shinya, Y. Hiruma and T. Takenaka, Ceram. Trans. 167 (2004) 310–329

25. A. Chaouchi, S. Kennour, S. d'Astorg, M. Rguiti, C. Courtois, S. Marinel, M. Aliouat, Journal of Alloys and Compounds 509 (2011) 9138– 9143.

26. M. Cerneaa, E. Andronescuc, R. Radua, F. Fochib, C. Galassib, Journal of Alloys and Compounds 490 (2010) 690–694.

27. K. Pengpat, S. Hanphimol, S. Eitssayeam, U. Intatha, G. Rujijanagul and T. Tunkasiri**,** Journal of Electroceramics 16 (2006) 301–305.

28. K.A. Razak, W.C. Song and C.Y. Ng, Procedia Chemistry 19 (2016) 816 – 821.

29. V. Pal, R.K. Dwivedi and O.P. Thakur, Current Applied Physics 14 (2014) 99107.

30. S.K. Acharya, B.G. Ahn, J.H. Hyung and S.K. Lee*,* Journal of the Korean Physical Society, 62 (2013) 794 799.

31. S.F. Wang, C.S. Tu, T.L. Chang, P.Y. Chen, C.S. Chen, V.H. Schmidt and J. Anthoniappen, Journal of Applied Physics 116 (2014) 154101.

32. R. Zuo, H. Wang, B. Ma and L. Li, Journal of Materials Science: Materials in Electronics 20 (2009) 1140–1143.

33. C. Zhou, X. Liu, W. Li and C. Yuan Materials Research Bulletin 44 (2009) 724.

34. K.N. Singh, V. Sao, P. Tamrakar, S. Soni, V.K. Dubey and P.K. Bajpai, Journal of Materials Science and Chemical Engineering, 3 (2015) 43-49.

35. Preeyakarn Eaksuwanchai and Methee Promsawat, Sukanda Jiansirisomboon and Anucha Watcharapasorn*,* Journal of the Korean Physical Society, 65 (2014) 377-381.

36. W.S. Kanga, S.K. Leeb and J.H. Koh, Ceramic International 1 (2015) 147.

37. J. Glaum, H. Simons, M. Acosta and M. Hoffman, Journal American Ceramic Society 96 (2013) 2881–2886.

38. M. Acosta, J. Zanga, W. Jo and J. Rödel, Journal of the European Ceramic Society 32 (2012) 4327–4334.

39. Z.M. Tian, Y.S. Zhang, S.L. Yuan, M.S. Wu, C.H. Wang, Z.Z. Ma, S.X. Huo, H.N. Duan, Materials Science and Engineering B 177 (2012) 74–78.

40. Y. Yuan, X.H. Zhou, C.J. Zhao, B. Li and S.R. Zhang, Journal of Electronic Materials 39 (2010) 11.

41. V.Q. Nguyen, H.S. Han, K.J. Kim, D.D. Dang, K.K. Ahnc and J.S. Leea, Journal of Alloys and Compounds 511 (2012) 237– 241.

42. M. Ehmke, J. Glaum, W. Jo, T. Granzow and J. Rodel, Journal American Ceramic Society 94 (2011) 2473–2478.

43. R. Selvamani, G. Singh, V.S. Tiwari, and P.K. Gupta, Physica Status Solidi A 209 (2012) 118–125.